VIP Electrocatalysis Very Important Paper

DOI: 10.1002/anie.201400358

Hollow Spheres of Iron Carbide Nanoparticles Encased in Graphitic Layers as Oxygen Reduction Catalysts**

Yang Hu, Jens Oluf Jensen, Wei Zhang, Lars N. Cleemann, Wei Xing, Niels J. Bjerrum, and Qingfeng Li**

Abstract: *Nonprecious metal catalysts for the oxygen reduction reaction are the ultimate materials and the foremost subject for low-temperature fuel cells. A novel type of catalysts prepared by high-pressure pyrolysis is reported. The catalyst is featured by hollow spherical morphologies consisting of uniform iron carbide (Fe_3C) nanoparticles encased by graphitic layers, with little surface nitrogen or metallic functionalities. In acidic media the outer graphitic layers stabilize the carbide nanoparticles without depriving them of their catalytic activity towards the oxygen reduction reaction (ORR). As a result the catalyst is highly active and stable in both acid and alkaline electrolytes. The synthetic approach, the carbide-based catalyst, the structure of the catalysts, and the proposed mechanism open new avenues for the development of ORR catalysts.*

Highly active and durable catalysts for the oxygen reduction reaction (ORR) are undoubtedly essential for the large-scale application of fuel cells.[1] The state-of-the-art catalyst is based on precious metals,[2] and the prohibitive costs, limited resources, and insufficient durability preclude commercialization of the technology.[1,2b,3] Accordingly, the development of cost-effective nonprecious metal catalysts (NPMCs) has been a foremost subject of the field.[4] Owing to the harsh ORR conditions especially in acidic media, only a few types of materials have been found to be active and durable towards the ORR, including, for example, carbon-supported transition-metal/nitrogen ($M{-}N_x/C$, M = Co, Fe, Ni, etc.) compounds,[5] metal-free nitrogen-doped carbon materials,[6] transition-metal chalcogenides.[7] Among the best is the $M{-}N_x/C$ catalyst where the active sites are believed to involve surface nitrogen coordinated with metals.[4]

Recently, a new type of NPMC based on Fe_3C has been reported to be active towards ORR. Wen et al.[8] synthesized nitrogen-enriched $Fe/Fe_3C{-}C$ nanorods as ORR catalysts in neutral media while Lee et al.[9] found that the Fe/Fe_3C-functionalized melamine foam exhibited good ORR activities in alkaline media. Though interesting, little information is known about the role of the Fe_3C phase in catalysis, probably because of two main reasons: first, the prepared Fe_3C-based catalysts were found to contain a certain amount of surface nitrogen,[8] indicating the possible presence of Fe_xN or/and N_xC sites. Second, the reported catalysts were a mixture of several phases, for example, carbon-coated Fe_3C in different scales, bare Fe_3C, and metallic Fe particles, making it difficult to conclude the role of the Fe_3C phase in the ORR. More critically, the possible use of the Fe_3C-based catalysts in acidic media is apparently out of question, as the carbide dissolves in acid.[10]

On the other hand, the $M{-}N_x/C$ catalysts prepared by pyrolysis are known to contain metal-rich particles encapsulated in graphitic carbon shells.[5a] And it is assumed that the encapsulation phases contribute little to the ORR activity.[11] However, as reported by Bao and co-workers in a series of studies,[12] when metal nanoparticles are confined inside carbon nanotubes (CNTs), a unique host–guest electronic interaction changes the local work function of the CNT walls. As a result, catalytic functionalities can be achieved on the outside surface of the CNTs. One example is the metallic iron nanoparticles confined within CNTs, which showed enhanced ORR activity compared to that of the pristine CNTs.[13]

Herein, in an attempt to prepare the $M{-}N_x/C$-type catalyst under high pressure, we expected to promote the formation of nitrogen functionalities. Instead we obtained a novel type of ORR catalyst with a negligible amount of nitrogen or metal on the surface. The catalyst shows well-controlled structures of hollow spheres comprising uniform Fe_3C nanoparticles encased by uniform graphitic layers. Because of the protection of the graphitic layers, the Fe_3C nanoparticles are chemically stable in hot acids. Towards the ORR the catalyst (hereafter referred to as Fe_3C/C) shows excellent activities and high stabilities in both acidic and alkaline media. More interestingly, the catalyst with the well-controlled structure and the negligible amount of nitrogen or iron on the surface provides a unique model material for probing the ORR active sites of the catalysts.

[*] M.Sc. Y. Hu, Dr. J. O. Jensen, Dr. L. N. Cleemann, Prof. N. J. Bjerrum, Dr. Q. F. Li
Department of Energy Conversion and Storage
Technical University of Denmark
Kemitorvet 207, 2800 Lyngby (Denmark)
E-mail: qfli@dtu.dk
M.Sc. Y. Hu, Prof. W. Xing
Laboratory of Advanced Power Sources
Changchun Institute of Applied Chemistry
Chinese Academy of Sciences, 130022, Changchun (China)
E-mail: xingwei@ciac.ac.cn
Dr. W. Zhang
Department of Energy Conversion and Storage
Technical University of Denmark
Risø campus, Frederiksborgvej 399, 4000, Roskilde (Denmark)

[**] This work was supported by the Danish National Research Foundation (Procon), Danish ForskEL (Catbooster), Danish Council for Strategic Research (4M Centre), and National Natural Science Foundation of China (grant number 21011130027). Dr. J. D. Zhang and Q. J. Chi, Department of Chemistry DTU, are thanked for assisting with the rotating ring disk electrode and helpful discussion.

Supporting information for this article is available on the WWW under http://dx.doi.org/10.1002/anie.201400358.

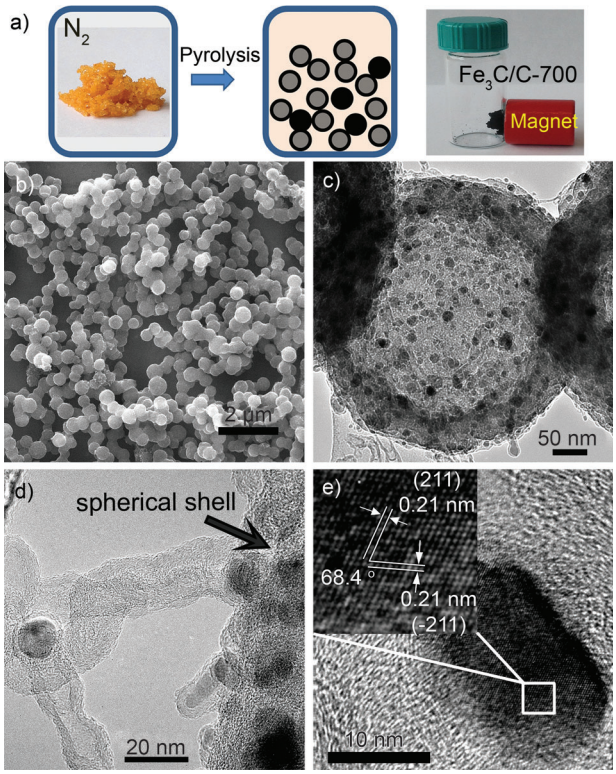

Figure 1. a) Synthesis of Fe_3C/C hollow spheres. b) SEM image of Fe_3C/C-700. c) TEM image of one typical hollow catalyst sphere of Fe_3C/C-700. d) TEM image of bamboo-like carbon nanotubes grown on the surface of the hollow spheres. e) HRTEM image of a Fe_3C nanoparticle in Fe_3C/C-700 and the index crystal plane shown in the inset.

As illustrated in Figure 1a, the Fe_3C/C hollow spheres were synthesized by one-step pyrolysis using ferrocene and cyanamide as precursors (see the Supporting Information). The synthesis was facile and, from more than 15 batches of the synthesis, a high reproducibility in terms of structure and performance was achieved. The obtained products were porous and magnetic powders along with a high-pressure gas phase. The structure of the typical catalyst Fe_3C/C-700 (as obtained from pyrolysis at 700 °C) is shown in Figure 1 as well as Figure S1–2 in the Supporting Information. The characteristic morphology is dimensionally uniform spheres with a diameter of 400–500 nm. As revealed by transmission electron microscopy (TEM) images (Figure S2a), a large proportion of these spheres are hollow spheres with a shell thickness of about 60 nm. A closer look at these spheres reveals that Fe_3C nanoparticles (about 10 nm in diameter) uniformly dispersed in the sphere structure. Around these spheres some Fe_3C nanoparticle-filled carbon nanotubes (CNTs) are observed, as shown in Figure 1d ad Figure S2. Focusing on the inner part of these hollow spheres, one can also distinguish some tube structures (Figure S2b). In the shell region of these spheres, high-resolution TEM (HRTEM) images (Figure S2d) show that the Fe_3C nanoparticles are coated by four to nine graphitic layers. These Fe_3C nanoparticles were checked by HRTEM analysis. As shown in Figure 1e for a typical nanoparticle, the spacing of crystalline lattices in two directions was both 0.21 nm with a characteristic angle of 68.4°, corresponding to the (−211) and (211) planes of the Fe_3C phase. The Fe_3C/C-800 catalyst (obtained from pyrolysis at 800 °C) showed a structure similar to that of Fe_3C/C-700 (Figure S3a). For catalysts and other materials prepared by pyrolysis, structure control is always a difficult task.[4a,9,14] This is particularly true for preparation of Fe_3C-based materials by pyrolysis.[10a,15] To the best of our knowledge, no Fe_3C with uniform morphology and evenly dispersed nanoparticles has been reported.

The bulk composition of the Fe_3C/C-700 catalyst was analyzed with energy dispersive X-ray spectroscopy (EDS), and X-ray diffraction (XRD) and thermogravimetric analysis (TGA). EDS (Figure 2a) shows that the catalyst contains C

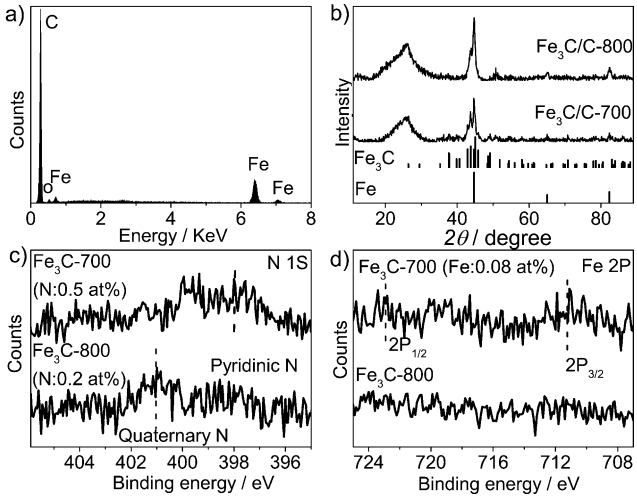

Figure 2. a) EDS spectrum of Fe_3C/C-700. b) XRD patterns of Fe_3C/C-700 and Fe_3C/C-800. c,d) High-resolution XPS N-1S (c) and Fe-2P (d) spectra of Fe_3C/C-700 and Fe_3C/C-800.

(ca. 82.1 wt %) and Fe (ca. 15.0 wt %) with a small amount of O (ca. 2.9 wt %). TGA measurement (Figure S4a) reveals an iron content of 15.8 wt % in Fe_3C/C-700, in good agreement with the EDS result. The XRD spectra confirm the presence of graphitic carbon atoms and a Fe_3C phase in Fe_3C/C-700. As shown in Figure 2b the broad peak of the XRD pattern at about 26.5° is indexed to the (002) planes of the graphitic carbon, while the other diffraction peaks were characteristic of Fe_3C (JCPDS 35-0772). Beside these two phases, the Fe_3C/C-800 sample contained traces of metallic iron (JCPDS 06-0696) (Figure 2b). The surface composition is of particular interest and the surface contents of N and Fe were examined by high-resolution X-ray photoelectron spectroscopy (XPS). As shown in Figure 2c, a trivial N-1s signal was observed for Fe_3C/C-700 (mainly from pyridinic N), signifying a negligible share of nitrogen atoms ($\leq$ 0.50 at %) on the catalyst surface. As to the Fe_3C/C-800 sample, the nitrogen content ($\leq$ 0.20 at %) was even smaller. Likewise, the Fe-2p spectra (Figure 2d) revealed a negligible surface iron content on the Fe_3C/C-700 ($\leq$ 0.08 at %) and the Fe_3C/C-800 (below detection limit). We have noticed the fact that XPS signals were noisy and tried to increase the number of scans, which however did not lead to any improvement unless for those

samples with higher elemental contents. Such low nitrogen and iron surface contents imply that the Fe_3C nanoparticles are exclusively encased by carbon layers in the catalysts. This structure was further verified by leaching the Fe_3C/C-700 sample in 0.5 M H_2SO_4 solution at 85 °C for 9 h. The resulting sample was named as Fe_3C/C-700L. Since the pure Fe_3C phase is soluble in acid, only protected by carbon layers can it survive in the leaching process. As shown in Figure 5a and Figure S3b, the corresponding XRD and TEM analyses for the Fe_3C/C-700L show little difference from the Fe_3C/C-700, revealing the well-preserved Fe_3C nanoparticles after the leaching process. Considering the use of a nitrogen-containing precursor, the surface nitrogen content for the obtained catalyst is surprisingly low, different from all previously reported catalysts prepared by pyrolysis under ambient pressure.[16] It seems the high pressure of pyrolysis is making the difference. The TGA (Figure S4b) demonstrates that both precursors are volatile and/or decomposed completely during pyrolysis, thus creating high pressure in the autoclave, which was estimated to be about 600 bar (see Supporting Information).

The ORR activities of Fe_3C/C catalysts were assessed in both acidic and alkaline solutions with the rotating disk electrode (RDE) and rotating ring disk electrode (RRDE) measurements (Figure 3). The results were compared with that of a commercial Pt/C catalyst. In 0.1 M $HClO_4$, the ORR polarization curve of Fe_3C/C-700 exhibited a high onset (ca. 0.90 V) and a half-wave potential (ca. 0.73 V), both about 0.1 V lower than that of Pt/C. The mass specific activity at 0.8 V was about 0.5 A g^{-1}, showing little dependence on the catalyst loadings on the RDE (see Figure 3e). This activity is comparable with the best MN_x/C catalysts reported.[4a,17] The H_2O_2 yield was found to be less than 8% at all potentials and decreased to about 6% at potentials below 0.6 V (Figure 3c), indicating a four-electron pathway dominated ORR process. Kinetic currents derived from the mass transport correction of the ORR currents (Figure 3f) show a Tafel slope of 59 mV per decade at low over-potentials, close to 57 mV per decade for the Pt/C catalyst. Therefore, similar to the ORR processes on Pt/C catalyst in acidic media, transfer of the first electron is probably the rate-determining step of the ORR for the Fe_3C/C catalysts.[18] To verify the chemical stability of the Fe_3C/C catalyst in acid for the ORR, the activity of the acid-leached Fe_3C/C-700L sample was also tested. It shows little change in the ORR activity compared with that for Fe_3C/C-700, indicating the catalytically active phase remained intact during the acid leaching process. The Fe_3C/C-800 catalyst showed a lower ORR activity than that of Fe_3C/C-700 in 0.1 M $HClO_4$ but a higher activity in 0.1 M KOH, just as good as the Pt/C catalyst (Figure 3b and Figure S5). The onset potentials and half-wave potentials were 1.05 and 0.83 V, respectively, for both Fe_3C/C-800 and Pt/C catalysts. The ORR of Fe_3C/C-800 in KOH involved a trivial H_2O_2 yield at low over-potentials but a high H_2O_2 yield (ca. 18%) in the diffusion-limiting current region (Figure 3d), indicating a different ORR mechanism in alkaline solution from that in acid. The ORR pathways in acidic or alkaline media were also assessed by an approach using the Koutecky–Levich equation, which showed similar results as those determined by RRDE

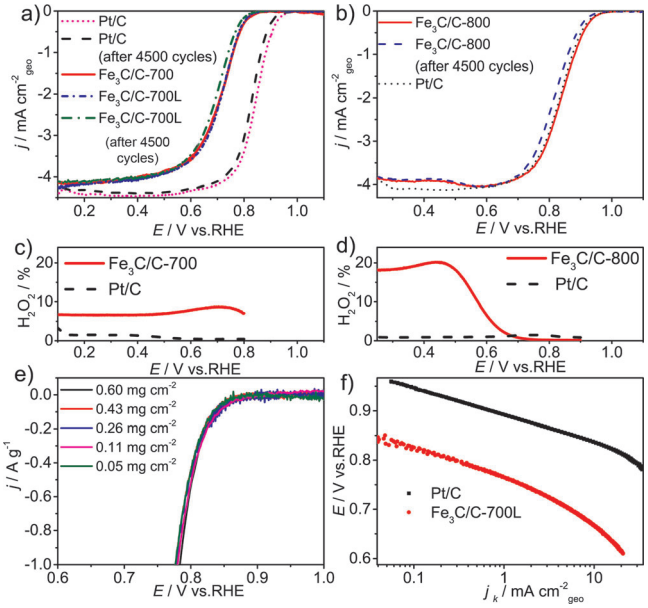

Figure 3. a) Linear sweep voltammograms (LSVs) of Fe_3C/C-700, Fe_3C/C-700L and Pt/C (20 wt% Pt on Vulcan XC-72, Johnson Matthey) at 900 rpm in O_2-saturated 0.1 M $HClO_4$ before and after 4500 potential cycles. Potential cycling was carried out between 0.6 and 1.0 V in N_2-saturated 0.1 M $HClO_4$. b) LSVs of Fe_3C/C-800 and Pt/C at 900 rpm in O_2-saturated 0.1 M KOH before and after 4500 potential cycles. Potential cycling was carried out between 0.6 and 1.0 V in N_2-saturated 0.1 M KOH. c) Peroxide yield of the Fe_3C/C-700 and Pt/C catalysts for the ORR in 0.1 M $HClO_4$. d) Peroxide yield of the Fe_3C/C-800 and Pt/C catalysts for the ORR in 0.1 M KOH. e) Mass-specific LSVs of Fe_3C/C-700 with different catalyst loadings on RDE at 900 rpm in O_2-saturated 0.1 M $HClO_4$. f) Tafel plots obtained from the RDE measurements on Fe_3C/C-700 and Pt/C at 900 rpm. The catalyst loading was 0.6 mg cm^{-2} for Fe_3C/C catalyst and 0.25 mg cm^{-2} (50 $\mu g_{(Pt)}$ cm^{-2}) for Pt/C catalyst. The scan rate was 10 mV S^{-1}.

measurements (Figure S6). Alongside the high ORR activity, Fe_3C/C catalysts showed also excellent methanol and H_3PO_4 tolerance for the ORR (Figure S7).

The ORR stability of the Fe_3C/C catalyst in acidic and alkaline media was evaluated using an accelerated durability test protocol.[19] As shown in Figure 3a and b, after 4500 potential cycles, the half-wave potentials for Fe_3C/C-700L in $HClO_4$ and Fe_3C/C-800 in KOH both shifted negatively by about 22 mV, similar to those for the Pt/C catalyst (16 mV in $HClO_4$ and 20 mV in KOH, Figure 3a and Figure S8a). Further extension of the stability test to 31500 cycles (140 h) in $HClO_4$ showed a small additional shift of the half-wave potential by 40 mV (Figure S8b). Chronoamperometric measurements were then carried out to confirm the stability, which showed even better stability of Fe_3C/C-800 in comparison with Pt/C (Figure S8c).

Concerning the nature of the ORR active sites, on one hand, the negligible surface nitrogen and iron content on the Fe_3C/C catalyst implies the fact that another mechanism instead of or in parallel to the well-recognized Fe–N_x and/or C–N_x active sites for the M–N_x/C-type catalysts might prevail for the ORR activity. Of particular note is a recent report by Ferrandon et al.[20] who showed that the presence of an Fe_3C

phase prohibited the Fe-N_4 active site formation during the pyrolysis. On the other hand, as discussed before and shown in Figure 4, the Fe_3C nanoparticles, which were encased by graphitic layers, are not in direct contact with the electrolyte or O_2, and hence not the direct ORR active sites.

To investigate the situation a destructive test of the Fe_3C/C catalyst was conducted by ball-milling to destroy the protective carbon shells around the carbide nanoparticles. The resulting sample was named as Fe_3C/C-700BL. After the milling, the Fe_3C nanoparticles were exposed and therefore soluble in hot acid during the following leaching. As revealed by XRD, SEM and TEM (Figure 5a and Figure S9), Fe_3C nanoparticles were largely removed after the milling-leaching process. Accordingly, it lost the magnetic property as well as the catalytic activity towards ORR. It seems clear that, despite the fact that the encased Fe_3C nanoparticles are not in direct contact with the electrolyte, they still play a key role in the catalysis. This role is most likely defined by the synergetic interaction between the carbide and protective graphitic layers. In other words, the encased carbide nanoparticles activate the surrounding graphitic layers, making the outer surface of the carbon layer active towards the ORR, as schematically illustrated in Figure 4.

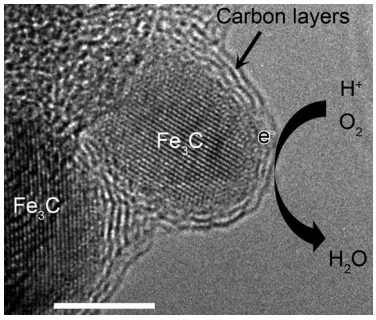

Figure 4. Oxygen reduction process on Fe_3C/C-700 (scale bar = 5.00 nm).

From previous work it was understood that nitrogen is a prerequisite for the active site formation of Fe-based ORR catalysts.[4a,21] To exclude the possible effect of nitrogen and its associated Fe–N_x or/and C–N_x species we attempted to synthesize the catalyst using nitrogen-free precursors. By doing so, any activity would be attributed to the catalytic nature of the carbon-surrounded Fe_3C particles. In the first synthesis, ferrocene was used as a single precursor (see the Supporting Information). As shown by XRD and TEM (Figure 5), the obtained sample (referred to as S1) was iron particles surrounded by thick carbon shells, and did not show more ORR activity than the Vulcan carbon black. This observation is in agreement with the previous report[21] that nitrogen-free precursors did not generate an ORR-active catalyst. However, this is not the case when a mixture of ferrocene and durene ($C_{10}H_{10}$) was used as nitrogen-free precursors. Thus obtained samples (referred to as S2-700 and S2-800 for samples prepared at 700 and 800 °C, respectively) possessed morphologies primarily consisting of carbon nano-

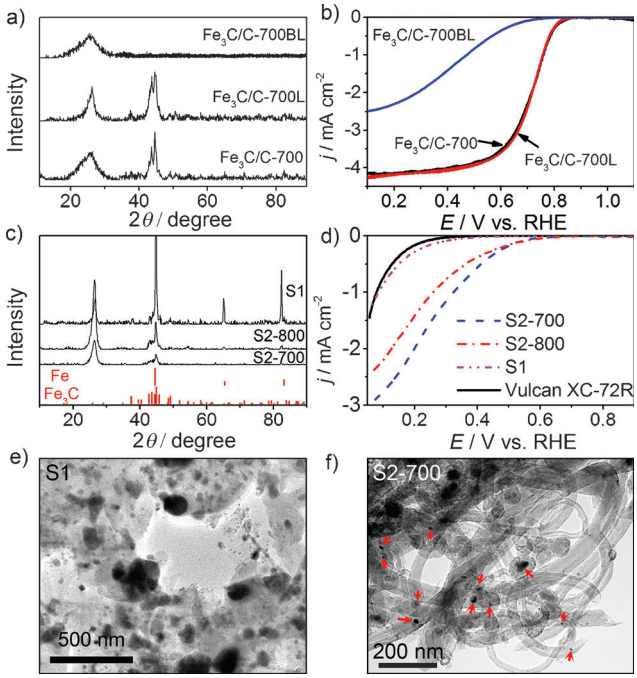

Figure 5. a) XRD patterns of Fe_3C/C-700, Fe_3C/C-700L, and Fe_3C/C-700BL. b) The corresponding ORR LSVs at 900 rpm in O_2-saturated 0.1 M $HClO_4$. The scan rate was 10 mV S^{-1}. c) XRD patterns of samples S1, S2-700, and S2-800 (see the Supporting Information for experimental details). d) ORR LSVs of Vulcan XC-72R, S1, S2-700, and S2-800 at 900 rpm in O_2-saturated 0.1 M $HClO_4$. The catalyst loadings were 0.6 mg cm^{-2} for all electrodes. e,f) TEM images of the samples S1 and S2-700. The arrows indicate the encapsulated Fe_3C particles.

tubes filled with Fe_3C particles (ca. 5 wt% of Fe by EDS, Figure 5 and Figure S10), similar to the previously described Fe_3C/C samples but not clustered in porous spheres. The S2 samples exhibited significant ORR activities in terms of onset potentials and reduction currents, though lower than those for the Fe_3C/C-700 catalyst, probably because of the different morphology and lower iron contents. This result clearly confirmed the ORR activity of the nitrogen-free catalyst and hence the assumed synergistic mechanism.

In summary, a novel ORR catalyst in form of hollow spheres comprising uniform Fe_3C nanoparticles encased by graphitic layers was synthesized by a one-step high-pressure pyrolysis process. The Fe_3C/C catalyst exhibited excellent ORR activity and stability in both acidic and alkaline media. With negligible surface nitrogen or iron functionalities, the catalyst is a model system for understanding the ORR active sites of this type of encapsulation catalysts. The outer protective graphitic layers stabilize the carbide nanoparticles in hot acids while the inner Fe_3C nanoparticles, though not in direct contact with the electrolyte, are proposed to play a synergetic role in activating the outer surface of the graphitic layers towards the ORR. The findings of the synthetic approach, the synthesized catalyst of the unique structure, and the proposed mechanism paves a way to further development of active and durable ORR catalysts for fuel cell applications.

Received: January 13, 2014
Published online: February 19, 2014

Keywords: electrocatalysis · fuel cells · iron carbides · nonprecious metal catalysts · oxygen reduction reaction

[1] a) B. C. H. Steele, A. Heinzel, *Nature* **2001**, *414*, 345 – 352; b) M. K. Debe, *Nature* **2012**, *486*, 43 – 51.
[2] a) T. Yu, D. Y. Kim, H. Zhang, Y. Xia, *Angew. Chem.* **2011**, *123*, 2825 – 2829; *Angew. Chem. Int. Ed.* **2011**, *50*, 2773 – 2777; b) A. Chen, P. Holt-Hindle, *Chem. Rev.* **2010**, *110*, 3767 – 3804.
[3] H. A. Gasteiger, S. S. Kocha, B. Sompalli, F. T. Wagner, *Appl. Catal. B* **2005**, *56*, 9 – 35.
[4] a) F. Jaouen, E. Proietti, M. Lefevre, R. Chenitz, J. P. Dodelet, G. Wu, H. T. Chung, C. M. Johnston, P. Zelenay, *Energy Environ. Sci.* **2011**, *4*, 114 – 130; b) Z. Chen, D. Higgins, A. Yu, L. Zhang, J. Zhang, *Energy Environ. Sci.* **2011**, *4*, 3167 – 3192.
[5] a) G. Wu, K. L. More, C. M. Johnston, P. Zelenay, *Science* **2011**, *332*, 443 – 447; b) M. Lefevre, E. Proietti, F. Jaouen, J. P. Dodelet, *Science* **2009**, *324*, 71 – 74.
[6] a) K. Gong, F. Du, Z. Xia, M. Durstock, L. Dai, *Science* **2009**, *323*, 760 – 764; b) S. Wang, L. Zhang, Z. Xia, A. Roy, D. W. Chang, J.-B. Baek, L. Dai, *Angew. Chem.* **2012**, *124*, 4285 – 4288; *Angew. Chem. Int. Ed.* **2012**, *51*, 4209 – 4212; c) R. L. Liu, D. Q. Wu, X. L. Feng, K. Mullen, *Angew. Chem.* **2010**, *122*, 2619 – 2623; *Angew. Chem. Int. Ed.* **2010**, *49*, 2565 – 2569.
[7] H. Wang, Y. Liang, Y. Li, H. Dai, *Angew. Chem.* **2011**, *123*, 11161 – 11164; *Angew. Chem. Int. Ed.* **2011**, *50*, 10969 – 10972.
[8] Z. Wen, S. Ci, F. Zhang, X. Feng, S. Cui, S. Mao, S. Luo, Z. He, J. Chen, *Adv. Mater.* **2012**, *24*, 1399 – 1404.
[9] J.-S. Lee, G. S. Park, S. T. Kim, M. Liu, J. Cho, *Angew. Chem.* **2013**, *125*, 1060 – 1064; *Angew. Chem. Int. Ed.* **2013**, *52*, 1026 – 1030.
[10] a) Y. Liao, K. Pan, L. Wang, Q. Pan, W. Zhou, X. Miao, B. Jiang, C. Tian, G. Tian, G. Wang, H. Fu, *ACS Appl. Mater. Interfaces* **2013**, *5*, 3663 – 3670; b) E. B. Easton, A. Bonakdarpour, R. Yang, D. A. Stevens, J. R. Dahn, *J. Electrochem. Soc.* **2008**, *155*, B547 – B557; c) Y. Hu, X. Zhao, Y. Huang, Q. Li, N. J. Bjerrum, C. Liu, W. Xing, *J. Power Sources* **2013**, *225*, 129 – 136; d) C. Giordano, A. Kraupner, I. Fleischer, C. Henrich, G. Klingelhofer, M. Antonietti, *J. Mater. Chem.* **2011**, *21*, 16963 – 16967.
[11] G. Faubert, R. Cote, J. P. Dodelet, M. Lefevre, P. Bertrand, *Electrochim. Acta* **1999**, *44*, 2589 – 2603.
[12] a) F. Zhang, X. Pan, Y. Hu, L. Yu, X. Chen, P. Jiang, H. Zhang, S. Deng, J. Zhang, T. B. Bolin, S. Zhang, Y. Huang, X. Bao, *Proc. Natl. Acad. Sci. USA* **2013**, *110*, 14861 – 14866; b) W. Chen, Z. Fan, X. Pan, X. Bao, *J. Am. Chem. Soc.* **2008**, *130*, 9414 – 9419.
[13] D. Deng, L. Yu, X. Chen, G. Wang, L. Jin, X. Pan, J. Deng, G. Sun, X. Bao, *Angew. Chem.* **2013**, *125*, 389 – 393; *Angew. Chem. Int. Ed.* **2013**, *52*, 371 – 375.
[14] E. Proietti, F. Jaouen, M. Lefèvre, N. Larouche, J. Tian, J. Herranz, J.-P. Dodelet, *Nat. Commun.* **2011**, *2*, 416.
[15] a) C. Giordano, A. Kraupner, S. C. Wimbush, M. Antonietti, *Small* **2010**, *6*, 1859 – 1862; b) Z. Schnepp, S. C. Wimbush, M. Antonietti, C. Giordano, *Chem. Mater.* **2010**, *22*, 5340 – 5344; c) J. N. Wang, L. Zhang, F. Yu, Z. M. Sheng, *J. Phys. Chem. B* **2007**, *111*, 2119 – 2124.
[16] a) H. T. Chung, C. M. Johnston, K. Artyushkova, M. Ferrandon, D. J. Myers, P. Zelenay, *Electrochem. Commun.* **2010**, *12*, 1792 – 1795; b) F. Charreteur, F. Jaouen, S. Ruggeri, J.-P. Dodelet, *Electrochim. Acta* **2008**, *53*, 2925 – 2938.
[17] F. Jaouen, J. Herranz, M. Lefevre, J. P. Dodelet, U. I. Kramm, I. Herrmann, P. Bogdanoff, J. Maruyama, T. Nagaoka, A. Garsuch, J. R. Dahn, T. Olson, S. Pylypenko, P. Atanassov, E. A. Ustinov, *ACS Appl. Mater. Interfaces* **2009**, *1*, 1623 – 1639.
[18] A. Kongkanand, S. Kuwabata, G. Girishkumar, P. Kamat, *Langmuir* **2006**, *22*, 2392 – 2396.
[19] Y. Li, W. Zhou, H. Wang, L. Xie, Y. Liang, F. Wei, J.-C. Idrobo, S. J. Pennycook, H. Dai, *Nat. Nanotechnol.* **2012**, *7*, 394 – 400.
[20] M. Ferrandon, A. J. Kropf, D. J. Myers, K. Artyushkova, U. Kramm, P. Bogdanoff, G. Wu, C. M. Johnston, P. Zelenay, *J. Phys. Chem. C* **2012**, *116*, 16001 – 16013.
[21] G. Lalande, R. Côté, D. Guay, J. P. Dodelet, L. T. Weng, P. Bertrand, *Electrochim. Acta* **1997**, *42*, 1379 – 1388.

